Characterization of the effect of ion irradiation on industrially produced GdBa$_2$Cu$_3$O$_{7-\delta}$ superconducting tapes using a slow positron beam

Atsushi Yabuuchi[1] *, Toshinori Ozaki[2], Hitoshi Sakane[3], Hiroyuki Okazaki[4], Hiroshi Koshikawa[4], Shunya Yamamoto[4], and Tetsuya Yamaki[4]

[1]*Institute for Integrated Radiation and Nuclear Science, Kyoto University, Kumatori, Osaka 590-0494, Japan*
[2]*Department of Nanotechnology for Sustainable Energy, Kwansei Gakuin University, Sanda, Hyogo 669-1337, Japan*
[3]*SHI-ATEX Co., Ltd., Saijo, Ehime 799-1393, Japan*
[4]*Takasaki Advanced Radiation Research Institute, National Institutes for Quantum and Radiological Science and Technology (QST), Takasaki, Gunma 370-1292, Japan*

To investigate the effect of irradiation-induced defects on the superconducting characteristics of industrially produced superconductor—GdBa$_2$Cu$_3$O$_{7-\delta}$ (GdBCO)—coated conductors (CCs), we irradiated the GdBCO CCs with Au ions at 2 or 10 MeV and probed them using a slow positron beam. Vacancy clusters were detected in both unirradiated and irradiated GdBCO CCs. However, the effect of ion irradiation on the GdBCO CCs was characterized as a slight reduction in the positron annihilation rate with low-momentum electrons. We also found a correlation between the annihilation rate of low-momentum electrons and the superconducting transition temperature.

A rare-earth-based cuprate superconductor—REBa$_2$Cu$_3$O$_{7-\delta}$ (REBCO)—exhibits high-temperature superconductivity and is expected to be useful for magnetic coils.[1,2] In order to employ REBCO-coated conductors (CCs) in superconducting magnetic coils, it is desirable to enhance the critical-current characteristics in high magnetic fields without degrading the superconducting transition temperature. Introducing lattice defects that pin the magnetic flux are shown to be effective for this purpose.[3] Ion irradiation enables the introduction of pinning centers with controlled concentrations and depth distributions without any modification of the deposition process. This is superior to the techniques of dispersing nanoparticles or self-assembled nanorods as pinning centers, where modifications of the deposition process are unavoidable. Many studies have therefore been performed to produce pinning centers using ion irradiation.[4–14]

Previous studies on enhancing the critical-current characteristics of REBCOs using ion irradiation have been conducted mainly by forming columnar defects using high-energy (> 100 MeV) heavy-ion irradiation.[4–10] However, enhancement of the critical-current characteristics also has been reported by irradiation with electrons,[15] neutrons,[16,17] protons,[11] or relatively low-energy (< 20 MeV) ions[12,13] that do not form columnar defects. This suggests that small defects, which are not visible even with a transmission electron microscope (TEM), contribute to the enhancement.[15] In addition, the concentration of vacancies formed by light-ion irradiation has been reported to be an important parameter in enhancing the critical-current characteristics of REBCO films.[12]

Positrons are sensitive to vacancy-type defects, and they are useful for characterizing irradiation-induced defects.[18–20] In this study, GdBa$_2$Cu$_3$O$_{7-\delta}$ (GdBCO) CCs, which were industrially produced with a roll-to-roll process, were irradiated with Au ions at 2 or 10 MeV and probed using a slow positron beam. The heavy Au-ion irradiation enables the formation of more vacancies with the same dosage in comparison with the light-ion irradiation, which is advantageous for mass produc-

tion.[13] Following such relatively low-energy Au-ion irradiation, no change was found in TEM observations. However, the experimental results showed that the photopeak of the 511 keV annihilation line was broadened by the ion irradiation, which was a contrary tendency to our initial expectation. Detailed measurements of the Doppler broadening of annihilation radiation (DBAR) spectra, and comparisons with calculated spectra, show that vacancy clusters are present in the industrially produced GdBCO CCs, even in the unirradiated state. Although this tendency was different from our initial expectation, we found a correlation between the decrease in the superconducting transition temperature (T_c) due to ion irradiation and the shape parameter (S-parameter) of the DBAR spectrum.

We utilized GdBCO CCs manufactured by Sumitomo Electric Industries—consisting of a composite metal tape, buffer layers, a superconducting layer (500 nm-thick GdBCO), and a silver stabilization layer—as samples. The GdBCO layer was deposited in a roll-to-roll process using a pulsed-laser-deposition technique. Details of the fabrication process are described elsewhere.[21] The buffer layers and the GdBCO layer were grown on an oriented metal substrate, and the grain size of the GdBCO was of the order of 100 μm, which is equivalent to the grain size of the metal substrate.[21] After fabrication, the topmost silver stabilization layer was removed by etching with a mixed solution of hydrogen peroxide and ammonia water.[21] In order to probe the samples with a slow positron beam, we arranged four GdBCO CCs, each 4 mm wide, side-by-side to form a set of 16×16 mm^2 samples.

We irradiated the 16 mm-square samples with 2 MeV Au^{2+} or 10 MeV Au^{4+} ions using the 3 MV tandem accelerator at the Takasaki Ion Accelerators for Advanced Radiation Application (TIARA) facility of the Takasaki Advanced Radiation Research Institute, QST. For each irradiation condition, we prepared two samples with different doses (low- and high-dose samples). The irradiation doses for each sample are listed in Table I. Figures 1(a) and (b) show the distributions of the ion stopping probability and of the displacement damage calculated with the SRIM-2008[22] code. The values of the displacement per atom (dpa) shown here are those for the high-dose

Table I. Irradiation doses for each sample.

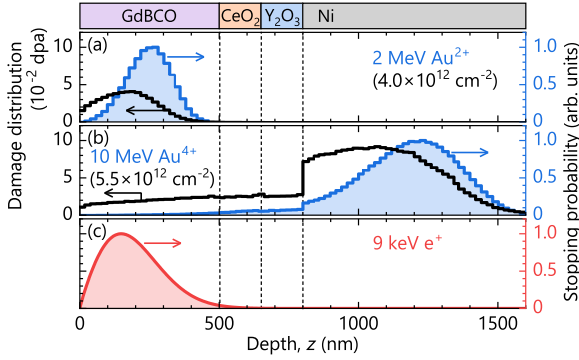| Ion and energy	Irradiation dose (cm^{-2})	
	Low-dose	High-dose
2 MeV Au^{2+}	5.0×10^{11}	4.0×10^{12}
10 MeV Au^{4+}	7.3×10^{11}	5.5×10^{12}

Fig. 1. Implantation distributions for (a) 2 MeV Au^{2+}, (b) 10 MeV Au^{4+}, and (c) 9 keV positrons. Panels (a) and (b) also show the damage distributions for the high-dose samples at each irradiation condition. The structure of the GdBCO samples is schematically shown at the top of the figure.

Fig. 2. S-parameters as functions of the incident positron energy for (a) 2 MeV Au^{2+} and (b) 10 MeV Au^{4+} irradiated GdBCO samples. All the S-parameters are normalized to that obtained from the GdBCO layer of the unirradiated sample (S_{unirr}). The upper horizontal axis denotes the mean implantation depth of positrons into GdBCO corresponding to the incident positron energy.

samples in each irradiation condition. For the 2 MeV Au^{2+} irradiation, the Au^{2+} ions stop in the GdBCO layer, and the peak of the displacement damage is also located in the GdBCO layer. In contrast, for the 10 MeV Au^{4+} irradiation, most of the Au^{4+} ions penetrate through the GdBCO layer and the buffer layers of CeO$_2$ and Y$_2$O$_3$ to reach the underlying metal substrate. Displacement damage caused by the 10 MeV Au^{4+} irradiation is nearly uniform throughout the GdBCO layer. After irradiation, the superconducting transition temperature T_c was determined from magnetization measurements using a superconducting quantum interference device (SQUID, Quantum Design) magnetometer.

All samples were then probed using a slow positron beam at the Kyoto University Research Reactor,[23–25] and the DBAR spectra were acquired with incident positron energies E_+ varying from 0.03 keV to 25 keV, using a high-purity germanium (HPGe, ORTEC GEM20-70) detector. The annihilation-radiation energy E_γ reflects the momentum of the annihilated electrons and is Doppler-shifted from 511 keV by $\pm\Delta E_\gamma = \pm c p_L/2$ (where c is the speed of light, and p_L is the longitudinal component of electron momentum along the direction of the gamma-ray emission).[26] The fraction of positrons annihilating with valence electrons increases when the positrons are trapped at vacancy-type defects. The increase in the fraction of positrons annihilating with valence electrons that have a narrow momentum distribution leads to a sharpening of the shape of the DBAR spectrum. The shape of the acquired DBAR spectra was characterized in terms of the S-parameter, which corresponds to annihilation with low-momentum electrons. This parameter is defined as the number of annihilation events over the energy range $|\Delta E_\gamma| \leq 0.77$ keV divided by the total number of annihilation events in the energy range $|\Delta E_\gamma| \leq 9.29$ keV. If the trapping fraction of positrons at defe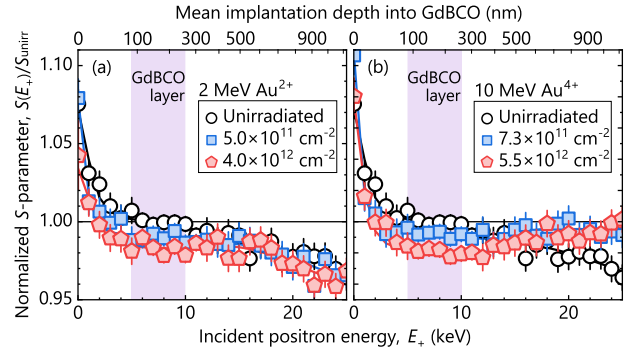cts is denoted by f, the observed S-parameter can be expressed as $S = (1 - f)S_B + f S_D$, where S_B and S_D are the values of S in the defect-free lattice (bulk) and in defects, respectively.[18] The measured S–E_+ plots were fitted using the VEPFIT[27,28] code.

In order to measure the momentum distributions of the annihilated electrons in detail, we also acquired coincidence DBAR[19,20,26] spectra using two HPGe detectors at E_+ = 9 keV for the unirradiated and the two high-dose samples. The stopping profile of positrons implanted into GdBCO at E_+ = 9 keV, calculated on the basis of a Makhovian profile,[29] is shown in Fig. 1(c). For comparison with the measured spectra, we calculated the theoretical DBAR spectra for all kinds of monovacancies in GdBCO using the first-principles calculation code ABINIT 8.10.3,[30] which is based on density-functional theory (DFT). In the calculations of the theoretical DBAR spectra, we modeled the electron-ion interaction using the projector augmented-wave method of Blöchl.[31,32] We used the generalized gradient approximation of Perdew, Burke, and Ernzerhoff[33] for the exchange-correlation functional between electrons. The positron annihilation calculations were performed using a two-component DFT scheme,[34] with the local-density approximation of Boroński and Nieminen[35] for the electron-positron exchange-correlation functional. The cutoff energy of the plane wave was 490 eV. The atomic configuration and positron-density distribution were obtained using the VESTA 3.4.6[36] code.

Figure 2 shows the S-parameters of the GdBCO samples before and after irradiation as functions of the incident positron energy. All the S-parameters are normalized to that of the GdBCO layer in the unirradiated sample (S_{unirr}) obtained from the VEPFIT analysis. The S-parameters for all irradiated samples show a clear reduction, compared with that for the unirradiated sample, in the incident positron-energy range 5–10 keV, where almost all positrons (> 96%) stop and annihilate in the GdBCO layer. This reduction in the S-parameters is opposite to the generally expected tendency of the S-parameter change caused by ion irradiation. The VEPFIT analysis also indicated that the positron-diffusion length L_+ is 9 nm, even in the unirradiated sample, which means that the effect of annihilation at the surface is negligible in the incident positron energy range 5–10 keV. In contrast, the 10 MeV Au^{4+} irradiated samples
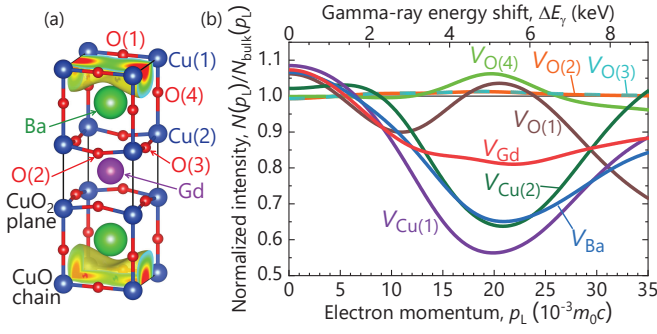
Fig. 3. (a) Crystalline structure and calculated positron-density distribution in defect-free GdBa$_2$Cu$_3$O$_7$. (b) Calculated DBAR spectra for all kinds of monovacancy sites in GdBCO. All the calculated spectra [$N(p_L)$] are normalized to the spectrum calculated for defect-free (bulk) GdBCO [$N_{bulk}(p_L)$]. The upper horizontal axis denotes the gamma-ray energy shift ΔE_γ corresponding to the annihilated electron momentum p_L.

Fig. 4. (a) Coincidence DBAR spectra obtained for unirradiated and high-dose samples at $E_+ = 9$ keV. The original measured spectra [$N(p_L)$] are normalized to the spectrum calculated for the defect-free (bulk) GdBa$_2$Cu$_3$O$_7$ lattice [$N_{bulk}(p_L)$]. The broken curves are spectra calculated for the monovacancies shown in Fig. 3(b).

Fig. 5. Normalized S-parameters in the GdBCO layer as a function of the superconducting transition temperature. The irradiation doses are indicated near each symbol in units of cm^{-2}. The shaded region is a guide to the eye.

show an increase in the S-parameters compared to the unirradiated state for $E_+ > 18$ keV. This increase may reflect the formation of vacancy-type defects in the buffer layers and/or in the metal substrate due to ion irradiation.

The reduction in the S-parameter after irradiation suggests that vacancy clusters larger in size than the irradiation-induced defects are present in the unirradiated state. To make the presence of the vacancy clusters more evident, we measured the coincidence DBAR spectra for the unirradiated and the two high-dose samples and compared them with the calculated spectra. Figure 3(b) shows the calculated DBAR spectra for all kinds of monovacancy sites in GdBCO. For example, V_{Gd} stands for a Gd vacancy, and the atomic sites corresponding to each subscript are identified in Fig. 3(a). The calculated positron-density distribution in defect-free orthorhombic GdBa$_2$Cu$_3$O$_7$ is also shown in Fig. 3(a). The delocalized positrons are concentrated between the CuO chains. Such a concentration of the positron distribution has also been reported for similar material YBa$_2$Cu$_3$O$_7$.[37,38] All the spectra shown in Fig. 3(b) are normalized to the spectrum calculated for defect-free GdBa$_2$Cu$_3$O$_7$. That is, the straight line $N(p_L)/N_{bulk}(p_L) = 1$ represents the DBAR spectrum for the defect-free lattice (bulk). For $V_{O(2)}$, $V_{O(3)}$, and $V_{O(4)}$, the momentum distribution of the annihilated electrons is almost the same as that of the defect-free lattice. However, for most of the vacancy sites, such as V_{Gd}, the intensity in the low-momentum region is higher than that of the defect-free lattice. In other words, because $|\Delta E_\gamma| \leq 0.77$ keV corresponds approximately to $|p_L| \leq 3 \times 10^{-3} m_0 c$, the S-parameter is increased compared to that of the defect-free lattice.

Figure 4 shows the coincidence DBAR spectra for the unirradiated and the high-dose samples normalized to the calculated defect-free GdBCO spectrum. As in Fig. 3(b), the straight line $N(p_L)/N_{bulk}(p_L) = 1$ represents the DBAR spectrum for the defect-free lattice. The dashed curves are the calculated spectra for the monovacancies shown in Fig. 3(b). The measured coincidence DBAR spectra show that the intensity in the low-momentum region ($|p_L| < 5 \times 10^{-3} m_0 c$) is even higher than those of all the calculated monovacancy spectra. In addition, the intensity in the high-momentum region ($|p_L| > 10 \times 10^{-3} m_0 c$) is even lower than those of all the calculated monovacancy spectra. This reflects an increase
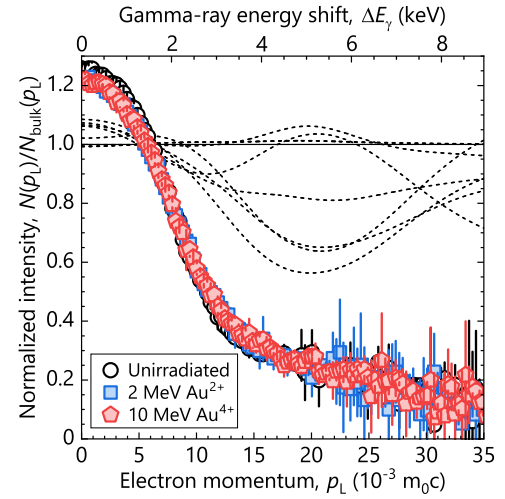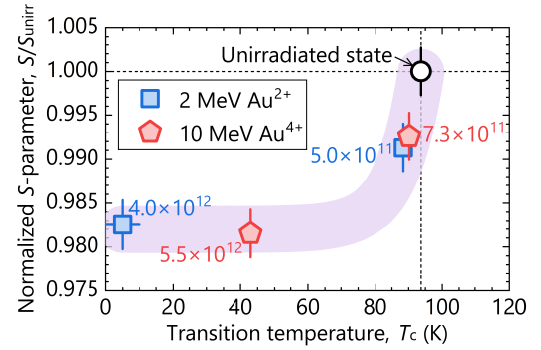
in the fraction of positrons that annihilate with valence electrons and a decrease in the fraction that annihilate with core electrons. Such features of the measured spectra indicate the presence of vacancy-type defects with sizes larger than those of the monovacancies (*i.e.*, vacancy clusters),[19] even in the unirradiated sample.

As shown in Fig. 4, vacancy clusters were detected in both the unirradiated and the irradiated samples from the coincidence DBAR measurements. Furthermore, the S-parameters were reduced by irradiating Au ions (Fig. 2). These results suggest that the mean size of vacancy-type defects is reduced by Au-ion irradiation. That is, the size of the newly-formed defects induced by the irradiation is smaller than that of the vacancy clusters initially contained in the samples.

Measurements of the superconducting transition temperature T_c show that the value of T_c decreased only a little for the low-dose samples, while the values of T_c for the high-dose samples decreased markedly. The relation between the S-parameter of the GdBCO layer obtained from the VEPFIT analysis and the value of T_c is plotted in Fig. 5. (Note that the 2 MeV Au^{2+} irradiated high-dose sample did not exhibit su-

perconductivity when it was measured at temperatures down to 10 K; thus, this sample is temporarily plotted in the figure at the position of 5 K with an error bar of ±5 K.) Even the low-dose samples with only slight decreases in T_c show significant reductions in the S-parameters. The S-parameters are further reduced in the high-dose samples that show marked decreases in T_c, but the reduction seems to be saturated at this dose level. Although Fig. 5 displays only a small number of plotted points, a correlation between the S-parameter and the value of T_c is found, indicating that irradiation-induced vacancy-type defects cause a reduction in T_c.

In this study, we focused on the correlation between the S-parameter and the value of T_c, and we investigated samples irradiated up to 10^{12} cm^{-2}, where the superconducting properties are markedly degraded. However, the critical-current density J_c in a magnetic field has already been found to be maximized at an irradiation dose in the mid-10^{11} cm^{-2} range.[13] Further studies to investigate the correlation between the S-parameter and the values of J_c are desired for samples with more finely varied doses up to the order of 10^{11} cm^{-2}. If a scaling relation is found between the S-parameter and the values of J_c, it would suggest that the vacancy-type defects induced by relatively low-energy ion irradiation, which are not visible in TEM observations, contribute to the enhancement of J_c.

In summary, although the tendency of the change we found was opposite to our initial expectation, we successfully characterized the effect of Au-ion irradiation on industrially produced GdBCO CCs by the change in the S-parameter. We also found a correlation between the S-parameter and the value of T_c, demonstrating that a slow positron beam can be a useful tool for characterizing the effects of ion irradiation on industrially produced superconducting CCs that contain vacancy clusters. Further studies using positrons are desired to clarify the relation between irradiation-induced defects and the enhancement of J_c.

Acknowledgements

1) Y. Shiohara, T. Taneda, and M. Yoshizumi, Jpn. J. Appl. Phys. **51**, 010007 (2012).
2) C. Senatore, M. Alessandrini, A. Lucarelli, R. Tediosi, D. Uglietti, and Y. Iwasa, Supercond. Sci. Technol. **27**, 103001 (2014).
3) K. Matsumoto and P. Mele, Supercond. Sci. Technol. **23**, 014001 (2010).
4) G. Isobe, M. Kiuchi, E. S. Otabe, T. Matsushita, S. Okayasu, and W. Prusseit, Physica C **468**, 1656 (2008).
5) T. Matsushita, G. Isobe, K. Kimura, M. Kiuchi, S. Okayasu, and W. Prusseit, Supercond. Sci. Technol. **21**, 054014 (2008).
6) T. Sueyoshi, T. Kotaki, Y. Uraguchi, M. Suenaga, T. Makihara, and T. Fujiyoshi, Physica C **530**, 72 (2016).
7) N. M. Strickland, S. C. Wimbush, P. Kluth, P. Mota-Santiago, M. C. Ridgway, J. V. Kennedy, N. J. Long, Nucl. Instrum. Methods Phys. Res., Sect. B **409**, 351 (2017).
8) E. I. Suvorova, P. N. Degtyarenko, I. A. Karateev, A. V. Ovcharov, A. L. Vasiliev, V. A. Skuratov, P. A. Buffat, J. Appl. Phys. **126**, 145106 (2019).
9) L. Liu, J. Liu, S. X. Zhang, J. Zeng, P. F. Zhai, P. P. Hu, L. J. Xu, Z. Z. Li, W. S. Ai, C. B. Cai, and M. J. Li, Appl. Phys. A **126**, 435 (2020).
10) T. Sueyoshi, T. Kotaki, Y. Furuki, T. Fujiyoshi, S. Semboshi, T. Ozaki, H. Sakane, M. Kudo, K. Yasuda, N. Ishikawa, Jpn. J. Appl. Phys. **59**, 023001 (2020).
11) Y. Jia, M. LeRoux, D. J. Miller, J. G. Wen, W. K. Kwok, U. Welp, M. W. Rupich, X. Li, S. Sathyamurthy, S. Fleshler, A. P. Malozemoff, A. Kayani, O. Ayala-Valenzuela, and L. Civale, Appl. Phys. Lett. **103**, 122601 (2013).
12) H. Matsui, T. Ootsuka, H. Ogiso, H. Yamasaki, M. Sohma, I. Yamaguchi, T. Kumagai, and T. Manabe, J. Appl. Phys. **117**, 043911 (2015).
13) M. W. Rupich, S. Sathyamurthy, S. Fleshler, Q. Li, V. Solovyov, T. Ozaki, U. Welp, W.-K. Kwok, M. Leroux, A. E. Koshelev, D. J. Miller, K. Kihlstrom, L. Civale, S. Eley, and A. Kayani, IEEE Trans. Appl. Supercond. **26**, 6601904 (2016).
14) H. Yamamoto, S. Ito, M. Miwa, S. Matsuyama, and H. Hashizume, J. Phys.: Conf. Ser. **1559**, 012045 (2020).
15) J. Giapintzakis, W. C. Lee, J. P. Rice, D. M. Ginsberg, and I. M. Robertson, Phys. Rev. B **45**, 10677 (1992).
16) J. Veterníková, M. Chudý, V. Slugeň, M. Eisterer, H. W. Weber, S. Sojak, M. Petriska, R. Hinca, J. Degmová, and V. Sabelová, J. Fusion Energ. **31**, 89 (2012).
17) M. Chudy, M. Eisterer, H. W. Weber, J. Veterníková, S. Sojak, and V. Slugeň, Supercond. Sci. Technol. **25**, 075017 (2012).
18) R. W. Siegel, Ann. Rev. Mater. Sci. **10**, 393 (1980).
19) F. Tuomisto, I. Makkonen, Rev. Mod. Phys. **85**, 1583 (2013).
20) J. Čížek, J. Mater. Sci. Technol. **34**, 577 (2018).
21) K. Ohki, T. Nagaishi, T. Kato, D. Yokoe, T. Hirayama, Y. Ikuhara, T. Ueno, K. Yamagishi, T. Takao, R. Piao, H. Maeda, and Y. Yanagisawa, Supercond. Sci. Technol. **30**, 115017 (2017).
22) J. F. Ziegler, Nucl. Instrum. Methods Phys. Res., Sect. B **219–220**, 1027 (2004).
23) Q. Xu, K. Sato, T. Yoshiie, T. Sano, H. Kawabe, Y. Nagai, K. Nagumo, K. Inoue, T. Toyama, N. Oshima, A. Kinomura, and Y. Shirai, J. Phys.: Conf. Ser. **505**, 012030 (2014).
24) K. Sato, Q. Xu, T. Yoshiie, T. Sano, H. Kawabe, Y. Nagai, K. Nagumo, K. Inoue, T. Toyama, N. Oshima, A. Kinomura, and Y. Shirai, Nucl. Instrum. Methods Phys. Res., Sect. B **342**, 104 (2015).
25) A. Yabuuchi, T. Yoshiie, and A. Kinomura, Nucl. Instrum. Methods Phys. Res., Sect. B **463**, 40 (2020).
26) P. Asoka-Kumar, M. Alatalo, V. J. Ghosh, A. C. Kruseman, B. Nielsen, and K. G. Lynn, Phys. Rev. Lett. **77**, 2097 (1996).
27) A. van Veen, H. Schut, J. de Vries, R. A. Hakvoort, and M. R. Ijpma, AIP Conf. Proc. **218**, 171 (1991).
28) A. van Veen, H. Schut, M. Clement, J. M. M. de Nijs, A. Kruseman, and M. R. Ijpma, Appl. Surf. Sci. **85**, 216 (1995).
29) P. J. Schultz and K. G. Lynn, Rev. Mod. Phys. **60**, 701 (1988).
30) X. Gonze, F. Jollet, F. Abreu Araujo, D. Adams, B. Amadon, T. Applencourt, C. Audouze, J.-M. Beuken, J. Bieder, A. Bokhanchuk, E. Bousquet, F. Bruneval, D. Caliste, M. Côté, F. Dahm, F. Da Pieve, M. Delaveau, M. Di Gennaro, B. Dorado, C. Espejo, G. Geneste, L. Genovese, A. Gerossier, M. Giantomassi, Y. Gillet, D. R. Hamann, L. He, G. Jomard, J. Laflamme Janssen, S. Le Roux, A. Levitt, A. Lherbier, F. Liu, I. Lukačević, A. Martin, C. Martins, M. J. T. Oliveira, S. Poncé, Y. Pouillon, T. Rangel, G.-M. Rignanese, A. H. Romero, B. Rousseau, O. Rubel, A. A. Shukri, M. Stankovski, M. Torrent, M. J. Van Setten, B. Van Troeye, M. J. Verstraete, D. Waroquiers, J. Wiktor, B. Xu, A. Zhou, and J. W. Zwanziger, Comput. Phys. Commun. **205**, 106 (2016).
31) P. E. Blöchl, Phys. Rev. B **50**, 17953 (1994).
32) G. Kresse and D. Joubert, Phys. Rev. B **59**, 1758 (1999).
33) J. P. Perdew, K. Burke, and M. Ernzerhof, Phys. Rev. Lett. **77**, 3865 (1996).
34) J. Wiktor, G. Jomard, M. Torrent, and M. Bertolus, Phys. Rev. B **87**, 235207 (2013).
35) E. Boroński and R. M. Nieminen, Phys. Rev. B **34**, 3820 (1986).
36) K. Momma and F. Izumi, J. Appl. Cryst. **44**, 1272 (2011).
37) S. Ishibashi, R. Yamamoto, M. Doyama, and T. Matsumoto, J. Phys.: Condens. Matter **3**, 9169 (1991).
38) M. Reiner, T. Gigl, R. Jany, G. Hammerl, and C. Hugenschmidt, Appl. Phys. Lett. **106**, 111910 (2015).